Numerical implementation of Asymmetric Mapping for Weak Singularities in High-Order Boundary Elements

JunHyung Jo[1*], and Yun Lee[2]

[1]*Korea Electric Power Corporation, Daegu Kyungbuk Construction Branch, Gong Pyeung Road 96, Junggu, Daegu, Republic of Korea*

[2]*Department of Civil Engineering, Daejeon University, 96-3 Yongun-dong, Dong-gu, Daejeon 300-716, Republic of Korea*

*Correspondence author : meta2phy@gmail.com (JunHyung Jo)

Abstract

This paper has discussed a cubic subparametric direct boundary element(CSDBE) formulation for linear elastic continuum, which is governed by the Lamé-Navier equation. asymmetric mapping technique is used to integrate the weak singularity term $U_{ij}(p,Q)$. The induced formulas are coded into a CSDBE and are verified by results of several examples, which are the simply connected region, the multiply connected region and the stress intensity problem. From a physical point of view, the simply connected region is the cantilever beam and the multiply connected region is the plate, which has one or more holes. The stress intensity problem is the double edge notched plate. The proposed numerical integration technique has yielded stable results. In addition, the effectiveness of degree of freedom is discussed through the examples. On the whole, a CSDBE is more effective than a linear boundary element using same the number of degree of freedoms. Considering the polynomial order used in the formulation, these results are natural. Meanwhile, the proposed numerical integration technique and formula derivation method can be used to realize the discontinuous boundary element used to satisfy the Hölder continuity.

Keywords : cubic subparametric direct boundary element, weak singularity, simply connected, multiply connected, effectiveness of degree of freedom, polynomial order, discontinuous boundary element, the Hölder continuity.

1. Introduction

The aims of this study are to construct Kernel integration technique, apply this technique to cubic subparametric direct boundary element method(CSDBEM) and evaluate robustness of it. In other words, the technique which this study determines provides detail way to construct high order subparametric direct boundary element method(HSDBEM). In addition, it is a secondary purpose to clarify the kernel integration method and construct an algorithm so that researchers interested in direct boundary element method(DBEM) can construct code and apply it to their work.

The linear equations of DBEM are generally harder than the FEM which is the main comparison object. The reason for this is briefly stated as the existence of fundamental solutions that limits the scope of the study, and the difficulty of calculating the singular integral within the fundamental solutions. In other words, it is connected to the ground of the birth of DBEM. In addition to the second of these, the coefficient matrix of the DBEM is composed of the product of the fundamental solution and the basis function, and the basic solution is composed of functions beyond general polynomial functions such as transcendental functions and rational functions[13, 14, 15, 16]. the product of the fundamental solutions and the basis functions should be integrated to construct the coefficient matrix. But the calculation of the specific integral at this time is relatively difficult. This is likely to prevent many people from accessing DBEM.

The singular integral that occurs when solving the 2D linear elastic problem with DBEM can be divided into weak singular integral, strong singular integral, and hyper singular integral [11, 12]. The calculation method and accuracy of these singular integrals will have a decisive influence on the level of solutions obtained through DBEM.

The subparametric elements mentioned above mean that the degree of function introduced to map the problem domain is lower than that of the basis function that forms the basis of the solution in the approximate analysis [6, 7]. The theory of subparametric elements is very simple, but it is not used well. This is because it is cumbersome to use two sets of basis functions in one code. However, this can be an alternative to reduce the computational complexity if the analytical shape such as the box culvert is simple square and the exterior is surrounded by semi-infinite ground. The subparametric DBEM was found in papers[6, 7, 8]. Particularly, discontinuous boundary elements have been used in the paper[8]. If the basis functions are inside of the element, generally, it becomes a discontinuous element[8].

For reference, the superparametric element is also used in DBEM. In particular, supposing that the basis of the solution is a constant, and using the mapping functions necessary for expressing the geometric shape of the analysis domain as the first order, the constant elements appear as superparametric elements very naturally. If the analysis domain is assumed to be a constant without assuming a linear function, there will be problems such as domain discontinuity and closed domain configuration.

In the case of a superparametric based DBEM,

assuming that the basis function of the solution is a constant, both the displacement value and the stress value appear discontinuously at the element boundary, similar to the solution of the finite element method.

Recently, papers on isogeometric modeling have been published on the topic of FEM [2, 3] as a study of matching the geometrical shape data and analytical data used in the CAD system by applying a change to the base function. Although FEM is mainly dealt with, in [4], a study has been carried out to use the NURBS curve as a basis function in the BEM by expressing the boundary shape. The NURBS used in the paper [4] is quadratic and cubic, controlled by knot vectors, and collocation points are used to construct linear equations. The collocation method is the way of determining the position of nodes by arbitrary or other methods when there are not characteristic positions in the basis function. In particular, [1] describes how to integrate NURBS used in isogeometric analysis

A study on the efficiency of BEM has also been carried out, and a thesis has been published [5] that measures efficiency by executing it with a GPU-based algorithm. In this paper, the efficiency of the GPU-based code for elastostatic problems was measured. GPUs introduced for the purpose of graphics processing have been greatly improved in recent years and are being developed in combination with CPUs. Especially, since it is a processor specialized for floating-point operations, it is expected to be widely used in high-end computing.

On the other hand, the subparametric BEM can be found in [7]. In this paper, high order hierarchical basis functions are used and linear equations using collocation method are constructed. And how to use high order basis functions and their usefulness have discussed [7].

In the field of kernel integration, research has also been published introducing methods for log integration in the kernel of isoparametric elements. In this study, new integration methods for quadratic and cubic elements were introduced without mentioning the overall composition of the BEM code and the analysis results [9]. In addition, numerical integration methods which can calculate cubic B-spline basis and logarithmically singular kernel have been presented and applied to FEM [10].

Many high-quality and valuable researches are conducted in each field. The mentioned papers are related to this study whether they are the same or opposite to the direction of this paper. However, these are very difficult for researchers who are new to it. So, as mentioned above, this study will concentrate on the application and implementation of easy-to-understand methods and their performance evaluation.

2. Direct boundary element method of Lamé-Navier equation

2.1 Lamé-Navier Equation and Kelvin Fundamental Solution

In this paper, the elasticity problem of the Lamé-Navier equation is the subject, and the expression of the problem is shown in eq. (1) [12, 14, 15]

$$(\lambda+\mu)\,u_{k,ki}+\mu\,u_{i,kk}+b_i=0 \quad (1)$$

A brief description of how to obtain the analytic solution of this problem is as follows. Applying the loading eq. (3) in the form of Dirac delta function to Lamé-Navier equation (1), Galerkin Vector G is used to make a biharmonic equation. The Kelvin solution (eqs (4, 5)) is then obtained by applying the solution of the Laplace equation twice in succession.

$$(\lambda+\mu)\,u_{k,ki}+\mu\,u_{i,jj}+\delta(p,Q)e_i=0 \quad (2)$$

$$b_j^*=\delta(p,Q)\boldsymbol{e}_i \quad (3)$$

$$u_j^*=u_{ij}^*(p,Q)\boldsymbol{e}_i \quad (4)$$

$$t_j^*=t_{ij}^*(p,Q)\boldsymbol{e}_i \quad (5)$$

2.2 Integral Equation of Direct BEM

These eqs. (3, 4, 5) is substituted into Maxwell-Betti's eq. (6) and finally the Somigliana Identity eq. (7) is derived. Somigliana Identity is an equation of integral form that can extract linear equations in DBEM, and it can be said that eq (8) corresponds to the weak form of finite element method. In eq (8) the source points p have been positioned on boundary of the domain. In eqs. (7, 8), P is source points of domain, p is source points on boundary and Q is field points. For the completeness of equations, the body force term has not been omitted in eqs. (7, 8). Eqs (9, 10) have showed tensor components t_{ij}^*, u_{ij}^* in 2-D problems.

$$\int_V b_i\,u_i^*dV+\int_\Gamma t_i\,u_i^*dS=\int_V b_i^*\,u_i dV+\int_\Gamma t_i^*\,u_i dS \quad (6)$$

$$1\times u_i(P)+\int_\Gamma t_{ij}^*(P,Q)u_j(Q)d\Gamma(Q)=\int_V u_{ij}^*(P,Q)b_j(Q)dV(Q)+\int_\Gamma u_{ij}^*(P,Q)t_j(Q)d\Gamma(Q) \quad (7)$$

$$C_{ij}(p)u_j(p)+\int_\Gamma t_{ij}^*(p,Q)u_j(Q)d\Gamma(Q)=\int_V u_{ij}^*(p,Q)b_j(Q)dV(Q)+\int_\Gamma u_{ij}^*(p,Q)t_j(Q)d\Gamma(Q) \quad (8)$$

$$t_{ij}^*(p,Q)=\begin{bmatrix}t_{xx}^*(p,Q) & t_{xy}^*(p,Q)\\ t_{yx}^*(p,Q) & t_{yy}^*(p,Q)\end{bmatrix} \quad (9)$$

$$u_{ij}^*(p,Q)=\begin{bmatrix}u_{xx}^*(p,Q) & u_{xy}^*(p,Q)\\ u_{yx}^*(p,Q) & u_{yy}^*(p,Q)\end{bmatrix} \quad (10)$$

3. Kernel Integration of Subparametric Element and and Construction of Linear equation

3.1 Subparametric Element

The subparametric DBEM to be implemented in this paper is assumed to be cubic polynomials (15 ~ 20) for basis functions approximating solutions and linear polynomials (11 ~ 14) for mapping functions.

All of the polynomials used in the research are Lagrange polynomials, which are the same as those used in the FEM and deal with the two-dimensional problem, but because of the characteristics of the BEM, one-dimensional functions are used [15, 17]. Fig. 1 and Fig. 2 show the mapping functions and basis functions used to construct cubic subparametric elements, respectively.

$$N_1^m = -\frac{1}{2}(\xi - 1) \quad (11) \qquad N_2^m = \frac{1}{2}(\xi + 1) \quad (12)$$

$$x = \sum_{i=1}^{2} N_i^m x_i \quad (13) \qquad y = \sum_{i=1}^{2} N_i^m y_i \quad (14)$$

$$\psi_1^c = \frac{9}{16}(1 - \xi)\left(\xi^2 - \frac{1}{9}\right) \quad (15)$$

$$\psi_2^c = \frac{27}{16}\left(\xi - \frac{1}{3}\right)(\xi^2 - 1) \quad (16)$$

$$\psi_3^c = \frac{27}{16}\left(\xi + \frac{1}{3}\right)(1 - \xi^2) \quad (17)$$

$$\psi_4^c = \frac{9}{16}(1 + \xi)\left(\xi^2 - \frac{1}{9}\right) \quad (18)$$

$$u = \sum_{i=1}^{4} \psi_i^c u_i \quad (19) \qquad v = \sum_{i=1}^{2} \psi_i^c v_i \quad (20)$$

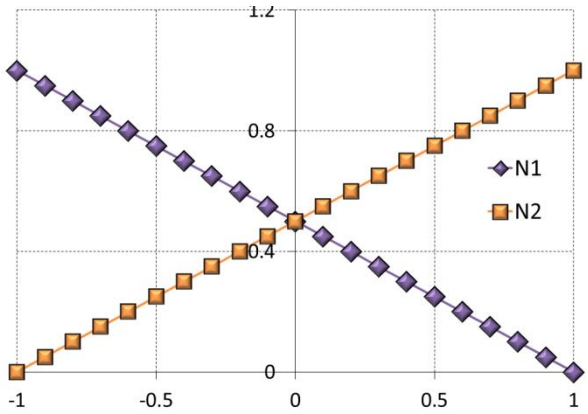

Fig. 1. Linear Lagrangian basis functions

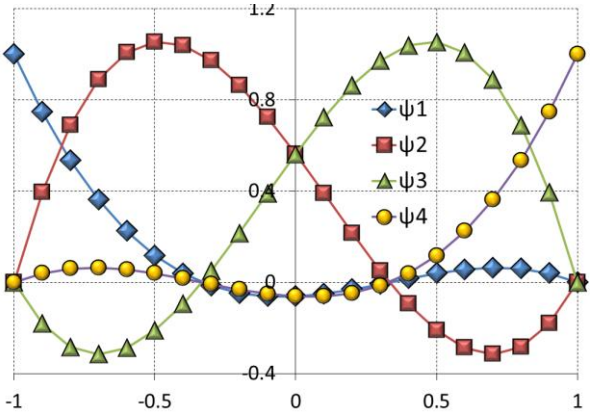

Fig. 2. Cubic Lagrangian basis functions

Fig. 3 represents the form in which the mapping function and base function are added together. Fig. 4 shows the model of boundary discretization using cubic subparametric elements.

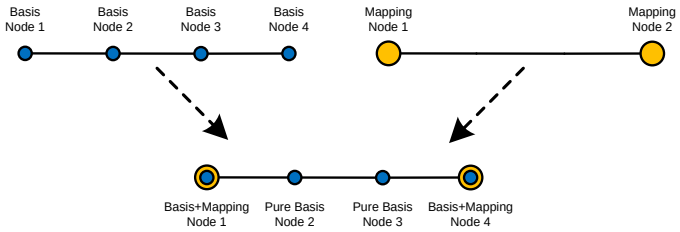

Fig. 3. Mapping Nodes, Basis Nodes, a Cubic subparametric element.

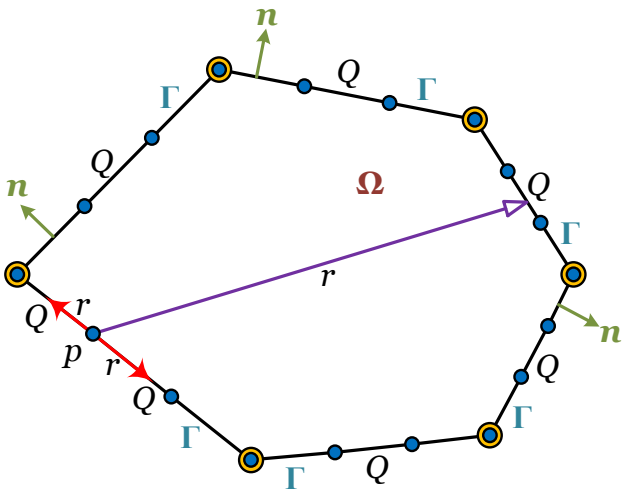

Fig. 4. Boundary discretization using cubic subparametric elements and r in the simply connected region

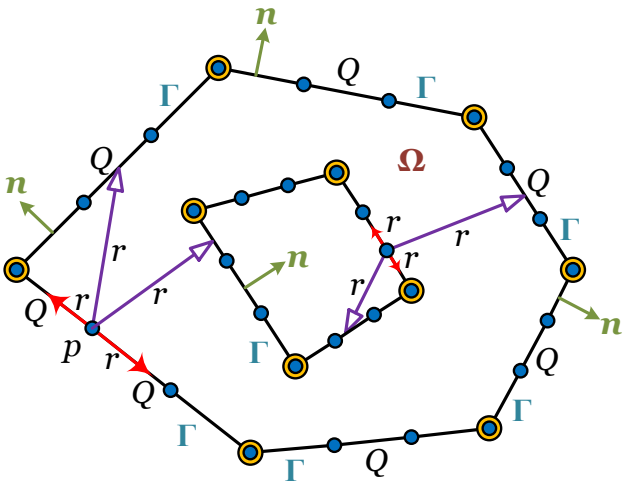

Fig. 5. Boundary discretization using cubic subparametric elements and r in the multiply connected region

If the basis function that approximates the solution is the first order, it is common to use the function of the same type and degree as the mapping function to simulate the domain. However, in the case of a curve boundary, the mapping region between nodes and nodes may not match the actual model. This phenomenon is inevitable when the first order element is used. Even if it is continuously refined, the error is reduced gradually and it does not disappear. As an alternative, a curve boundary is discretized using a higher order element of degree 2, and at the same time, the basis function space of the solution is expanded to increase the accuracy of the approximate solution. However, there is the possible side effect that virtual curved boundary can be analyzed except actual curved boundary. Also, if straight line boundaries are analyzed, the use of curve mapping is accompanied by a slight increase in unnecessary computation and slight oscillation of solutions. In this case, it will have bad influences on the final solution.

Considering the above problem, the benefits of using higher order isoparametric elements to improve the solution cannot be found other than the increase in the basis function space of the solution. In conclusion, subparametric elements result in an alternative to take only the merit of increasing the basis function space of the solution in problems of straight line boundaries.

3.2 Asymmetric Mapping for Kernel Integration

In order to implement CSDBEM, it is very important to calculate the singular integration value using linear mapping. $U_{ij}(p,Q)$ appears on the right side of eq. (21) and contains the ln function. The variable in the ln is $\frac{1}{r}$, which is the reciprocal of the distance from the source points to the field points of the boundary where the problem is defined. Therefore, if r is 0, $\frac{1}{r}$ is calculated as ∞. So $ln\left(\frac{1}{r}\right)$ is singular. Or if $-ln(r)$ is calculated, 0 is assigned to r, and $ln(r)$ is -∞, a singular integral.

This singular integral exists, but cannot be calculated by Gaussian numerical integration, and is integrated using a logarithmic numerical integral. Especially, when integrating the integrand as it is, the result is calculated incorrectly. Therefore, it is necessary to divide into a singular integrand part and a normal integrand part. Without this division process, the value of eq. (21) is still incorrectly calculated even if logarithmic numerical integration is used.

Thus, the singularity within $u_{ij}^*(p,Q)$ is called the weak singular. On the other hand, $t_{ij}^*(p,Q)$ has the strong singularity in the inside of eq. (22). In this case, we can use the diagonal matrix formula eq. (64) that takes into account rigid body motion. Usually the Cauchy principal value integral should be used to analysis the more general problems.

$$u_{ij}^*(p,Q) = \frac{1}{8\pi\mu(1-\nu)}\left[(3-4\nu)\,ln\frac{1}{r}\delta_{ij} + r_{,i}\,r_{,j}\right] \quad (21)$$

$$t_{ij}^*(p,Q) = \frac{-1}{4\pi(1-\nu)r}\left[\{(1-2\nu)\delta_{ij} + 2r_{,i}\,r_{,j}\}r_{,n} - (1-2\nu)\left(r_{,i}\,n_{,j} - r_{,j}\,n_{,i}\right)\right] \quad (22)$$

When using the linear mapping functions as in eqs. (11, 12), since the number of nodes representing the mapping functions and the number of nodes representing the basis functions, eqs (15 ~ 18) are two and four respectively, the interior nodes are related only to the solution, but unrelated to the mapping. Therefore, these nodes are called pure basis nodes, and they are regarded as source points to make linear equations. The integration is performed for all boundaries about these source points.

In such a case, it is a general technique to calculate by introducing a mode, which is the degree of freedom of the function, doesn't have specific location and multiplied over the function as a whole in the FEM[6, 7]. However, due to the nature of BEM, in other words, the physical distance to the kernel function is included as a variable. In order to satisfy this requirement, a degree of freedom of which the position should be determined, that is, a physical node is required. Since characteristics of this node are different from the characteristics of mode. It is defined as a pure basis node. In some cases, arbitrary points are selected, which are called collocation points[4, 6].

In this paper, the positions of the pure basis nodes have be selected as -1/3 and 1/3, which are the positions where the function value is 1 in the four elements of the Lagrange basis function. This is because, if the basis function value is 1 (unit value) at the corresponding node position, the unknown values of the corresponding node in the linear equations can be recognized as direct solutions without additional interpolation calculations. However, there is no

rule that the node should be determined at the position of the basis function value 1, and the arbitrary positions may be determined as the physical position of the nodes. In this case, additional calculations must be performed to determine the physical values at the nodal points, such as displacements and stresses. Otherwise, it is possible to newly derive the basis functions value to be 1 at the changed node position [11, 12, 17].

Each source point is located at a position corresponding to the basis function value 1 represented by the polynomials (15 ~ 18), and source points are all four points. The equation for calculating the distance between the element and each source points is a formula for calculating the distance between the source point and the Gauss integration point, since the numerical integration should be performed chapter. 3.1.1 to chapter 3.1.4 contain the distance equation, which must always be calculated differently depending on how the mapping function is determined, the process of separating singular terms, and integrating the singular values by assigning these equations to the integrand.

Node 1, 4 can be integrated by only one mapping. However, it is possible to integrate boundaries for nodes 2 and 3 by performing mapping twice in the regular interval [-1, 1]. This mapping section has an asymmetric shape on the center of the regular interval [-1, 1]. When the source point is located at 0, the two sections [-1. 0] and [0, 1] are symmetrical, and the expression becomes very simple.

The method shown above is expressed as an explicit integral for each interval in the following section. The main difference between the subparametric and isoparametric elements is the change in the integration process due to the nodal difference between the mapped function and the basis function.

3.2.1 Node 1 [-1, 1] Interval Integration

$$r^2(p,Q) = \left(\sum_{i=1}^{2} N_i^m x_i - x_1\right) + \left(\sum_{i=1}^{2} N_i^m y_i - y_1\right) \quad (23)$$

$$= \left\{-\frac{1}{2}(\xi+1)\right\}^2 \{(x_1-x_4)^2 + ((y_1-y_4)^2)\} \geq 0 \quad (24)$$

$$\xi \in [-1,1] \longrightarrow \eta \in [0,1] \implies \eta = -\frac{1}{2}(\xi+1) \quad (25)$$

$$\int_\Gamma u_{ij}^*(p,Q)t_j(Q)d\Gamma(Q) =$$

$$\int_{-1}^{1} \frac{(3-4\nu)}{8\pi(1-\nu)\mu}\delta_{ij}\left\{ln\left(\frac{1}{\left|-\frac{1}{2}(\xi+1)\right|}\right)-\frac{1}{2}ln(l_e^2)\right\} + \frac{1}{8\pi(1-\nu)\mu} r_{,i}\, r_{,j}\, \boldsymbol{\psi}(\xi)\boldsymbol{J}d\xi \quad (26)$$

$$\int_{-1}^{-\frac{1}{3}} \frac{(3-4\nu)}{8\pi(1-\nu)\mu}\delta_{ij}\left\{ln\left(\frac{1}{\left|-\frac{1}{2}(\xi+1)\right|}\right)\right\}\boldsymbol{\psi}(\xi)\boldsymbol{J}d\xi$$

$$\rightarrow \int_0^1 \frac{(3-4\nu)}{8\pi(1-\nu)\mu}\delta_{ij}\left\{ln\left(\frac{1}{|-\eta|}\right)\right\}\boldsymbol{\psi}(\xi)\boldsymbol{J}|\boldsymbol{2}|d\eta \quad (27)$$

$$\int_{-1}^{-1} \frac{(3-4\nu)}{8\pi(1-\nu)\mu}\delta_{ij}\left(-\frac{1}{2}\right) l\, n(l_e^2)\, \boldsymbol{\psi}(\xi)\boldsymbol{J}d\xi \quad (28)$$

$$\int_{-1}^{-1} \frac{1}{8\pi(1-\nu)\mu} r_{,i}\, r_{,j}\, \boldsymbol{\psi}(\xi)\boldsymbol{J}d\xi \quad (29)$$

These formulas are detailed expressions for numerical calculation. Expression (27) is the logarithmic numerical integration, and expressions (28) and (29) are the Gaussian numerical integration. At this time, Jacobian is calculated using the first order basis function used for the subparametric elements. Expressions (28) and (29) consistently designate because they are the same shape but have different interval of integration for the following each node.

3.2.2 Node 2 Integration

$$r^2(p,Q) = \left(\sum_{i=1}^{2} N_i^m x_i - x_2\right) + \left(\sum_{i=1}^{2} N_i^m y_i - y_2\right) \quad (30)$$

$$= \left\{-\frac{1}{2}\left(\xi+\frac{1}{3}\right)\right\}^2 \{(x_1-x_4)^2 + ((y_1-y_4)^2)\} \geq 0 \quad (31)$$

$$\int_\Gamma u_{ij}^*(p,Q)t_j(Q)d\Gamma(Q) =$$

$$\int_{-1}^{+1} \frac{(3-4\nu)}{8\pi(1-\nu)\mu}\delta_{ij}\left\{ln\left(\frac{1}{\left|\frac{1}{2}\left(\xi+\frac{1}{3}\right)\right|}\right)-\frac{1}{2}ln(l_e^2)\right\} + \frac{1}{8\pi(1-\nu)\mu} r_{,i}\, r_{,j}\, \boldsymbol{\psi}(\xi)\boldsymbol{J}d\xi \quad (32)$$

As before, it is divided into three expressions for convenience, and the interval of integration is decisively divided into $\left[-1,-\frac{1}{3}\right],\left[-\frac{1}{3},1\right]$ and separated into two terms again. A schematic diagram is shown in Fig. 6.

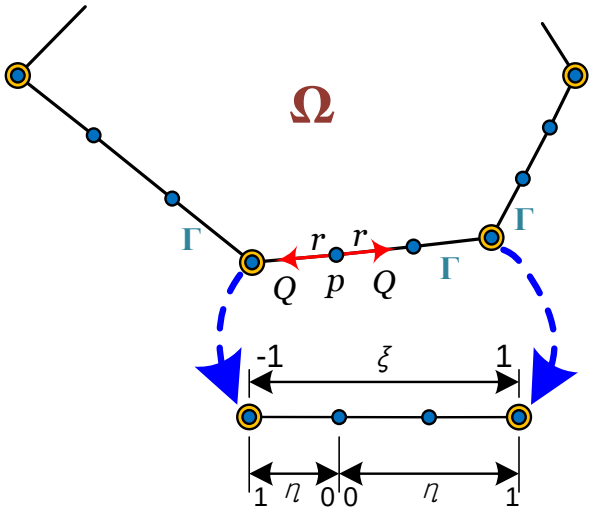

Fig. 6. Node 2 mapping interval for integration

3.2.2.1 $\left[-1,-\frac{1}{3}\right]$ Interval Integration of Node 2

$$\xi \in \left[-1,-\frac{1}{3}\right] \rightarrow \eta \in [1,0] \Rightarrow \eta = -\frac{1}{2}(3\xi+1) \quad (33)$$

$$\int_{\Gamma} u_{ij}^{*}(p,Q)t_j(Q)d\Gamma(Q) =$$

$$\int_{-1}^{-\frac{1}{3}} \frac{(3-4\nu)}{8\pi(1-\nu)\mu}\delta_{ij}\left\{ln\left(\frac{1}{\left|\frac{1}{2}\left(\xi+\frac{1}{3}\right)\right|}\right)-\frac{1}{2}ln(l_e^2)\right\} + \frac{1}{8\pi(1-\nu)\mu}r_{,i}\,r_{,j}\,\boldsymbol{\psi}(\xi)\boldsymbol{J}d\xi \quad (34)$$

$$\int_{-1}^{-\frac{1}{3}} \frac{(3-4\nu)}{8\pi(1-\nu)\mu}\delta_{ij}\left\{ln\left(\frac{1}{\left|\frac{1}{2}\left(\xi+\frac{1}{3}\right)\right|}\right)\right\}\boldsymbol{\psi}(\xi)\boldsymbol{J}d\xi \rightarrow \int_{0}^{1} \frac{(3-4\nu)}{8\pi(1-\nu)\mu}\delta_{ij}\left\{ln\left(\frac{1}{\left|-\frac{1}{3}\right|}\right) + ln\left(\frac{1}{|\eta|}\right)\right\}\boldsymbol{\psi}(\xi)\boldsymbol{J}\left|-\frac{\boldsymbol{2}}{\boldsymbol{3}}\right|d\eta \quad (35)$$

$$\int_{-1}^{-\frac{1}{3}} \frac{(3-4\nu)}{8\pi(1-\nu)\mu}\delta_{ij}\left(-\frac{1}{2}\right)l\,n(l_e^2)\,\boldsymbol{\psi}(\xi)\boldsymbol{J}d\xi \quad (36)$$

$$\int_{-1}^{-\frac{1}{3}} \frac{1}{8\pi(1-\nu)\mu}r_{,i}\,r_{,j}\,\boldsymbol{\psi}(\xi)\boldsymbol{J}d\xi \quad (37)$$

After transforming expression (35) from the left to the right, the Gaussian numerical integration interval [0, 1] should be performed and the logarithmic numerical interval [0, 1] should be performed in the following term.

The right terms are the expression (35) that a singular term is separated from left terms of expression (35). In particular, the ratio of the interval between ξ and η $\left|-\frac{2}{3}\right|$ is as follows. This value is defined as pseudo Jacobian. This value was derived by mapping with corresponding the location of the singular values of the original integral interval $\left[-1,-\frac{1}{3}\right]$ to the regular integral interval $[1,0]$. That is, the positions of the beginning and end of the original integral interval $\left[-1,-\frac{1}{3}\right]$ and the regular integral interval $[1,0]$ change. Therefore, the ratio is calculated as $d\xi = -\frac{2}{3}d\eta$, but always has a positive value for the integration. As an expression is following, $\int_{-1\rightarrow 1}^{-\frac{1}{3}\rightarrow 0} f(\xi)d\xi = -\int_{-1\rightarrow 1}^{-1\rightarrow 1} f(\xi)d\xi = -\int_{-\frac{1}{3}\rightarrow 0}^{-1\rightarrow 1} f(\eta(\xi))d\eta = -\int_{0}^{1} f(\eta(\xi))\left(-\frac{2}{3}\right)d\eta \overset{\text{def}}{=} \int_{0}^{1} f(\eta(\xi))\left|-\frac{2}{3}\right|d\eta$. Finally, the integral value is obtained by adding the expressions (35), (36) and (37). The expressions (36) and (37) are calculated by using Gaussian numerical integration.

3.2.2.2 $\left[-\frac{1}{3},1\right]$ Interval Integration of Node 2

$$\xi \in \left[-\frac{1}{3},1\right] \rightarrow \eta \in [0,1] \Rightarrow \eta = \frac{1}{4}(3\xi+1) \quad (38)$$

$$\int_{\Gamma} u_{ij}^{*}(p,Q)t_j(Q)d\Gamma(Q) =$$

$$\int_{-\frac{1}{3}}^{1} \frac{(3-4\nu)}{8\pi(1-\nu)\mu}\delta_{ij}\left\{ln\left(\frac{1}{\left|\frac{1}{2}\left(\xi+\frac{1}{3}\right)\right|}\right)-\frac{1}{2}ln(l_e^2)\right\} + \frac{1}{8\pi(1-\nu)\mu}r_{,i}\,r_{,j}\,\boldsymbol{\psi}(\xi)\boldsymbol{J}d\xi \quad (39)$$

$$\int_{-\frac{1}{3}}^{1} \frac{(3-4\nu)}{8\pi(1-\nu)\mu}\delta_{ij}\left\{ln\left(\frac{1}{\left|\frac{1}{2}\left(\xi+\frac{1}{3}\right)\right|}\right)\right\}\boldsymbol{\psi}(\xi)\boldsymbol{J}d\xi \rightarrow \int_{0}^{1} \frac{(3-4\nu)}{8\pi(1-\nu)\mu}\delta_{ij}\left\{ln\left(\frac{1}{\left|\frac{\boldsymbol{2}}{\boldsymbol{3}}\right|}\right) + ln\left(\frac{1}{|\eta|}\right)\right\}\boldsymbol{\psi}(\xi)\boldsymbol{J}\left|\frac{\boldsymbol{4}}{\boldsymbol{3}}\right|d\eta \quad (40)$$

$$\int_{-\frac{1}{3}}^{1} \frac{(3-4\nu)}{8\pi(1-\nu)\mu}\delta_{ij}\left(-\frac{1}{2}\right)l\,n(l_e^2)\,\boldsymbol{\psi}(\xi)\boldsymbol{J}d\xi \quad (41)$$

$$\int_{-1}^{-\frac{1}{3}} \frac{1}{8\pi(1-\nu)\mu}r_{,i}\,r_{,j}\,\boldsymbol{\psi}(\xi)\boldsymbol{J}d\xi \quad (42)$$

The mapping for Node 2 is asymmetric around 0 in expressions (33 ~ 37) and expressions (38 ~ 42), and is performed on both sides. This section adjoins the previous integral interval $\left[-1,-\frac{1}{3}\right]$. Therefore, this method is called asymmetric mapping. The same procedure is repeated for the successive Node 3. However, for the sake of completeness of formulas, all expressions are shown without omission. If calculation efficiency is to be sought, the

expressions (36) and (37) in 3.2.2.1 and the expressions (39 41) and (40 42) in 3.2.2.2 can be obtained by applying a Gaussian numerical integration of the interval [-1, 1] simultaneously.

3.2.3 Node 3 Integration

$$r^2(p,Q) = \left(\sum_{i=1}^{2} N_i^m x_i - x_3\right) + \left(\sum_{i=1}^{2} N_i^m y_i - y_3\right) \quad (43)$$

$$= \left\{-\frac{1}{2}\left(\xi + \frac{1}{3}\right)\right\}^2 \{(x_1 - x_4)^2 + ((y_1 - y_4)^2)\} \geq 0 \quad (44)$$

$$\int_\Gamma u_{ij}^*(p,Q) t_j(Q) d\Gamma(Q) =$$

$$\int_{-1}^{1} \frac{(3-4\nu)}{8\pi(1-\nu)\mu} \delta_{ij} \left\{ ln\left(\frac{1}{\left|\frac{1}{2}\left(\xi - \frac{1}{3}\right)\right|}\right) - \frac{1}{2} ln(l_e^2) \right\} + \frac{1}{8\pi(1-\nu)\mu} r_{,i} r_{,j} \psi(\xi) J d\xi \quad (45)$$

As before, it is divided into three expressions for convenience, and the interval of integration is decisively divided into $\left[-1, \frac{1}{3}\right], \left[\frac{1}{3}, 1\right]$ and separated into two terms again. A schematic diagram is shown in Fig. 7.

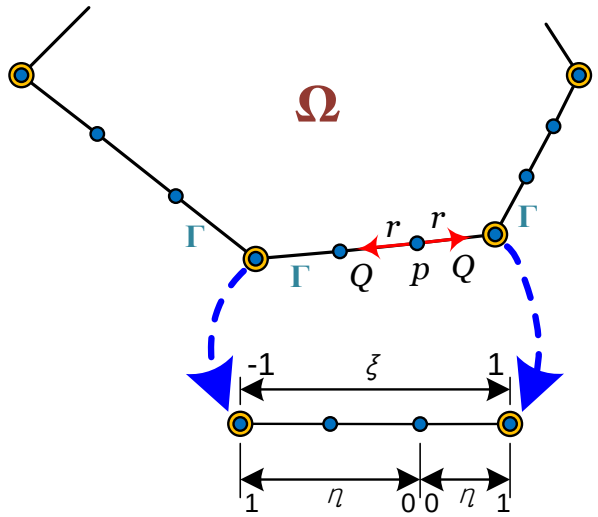

Fig. 7. Node 3 mapping interval for integration

3.2.3.1 $\left[-1, \frac{1}{3}\right]$ Interval Integration of Node 3

$$\xi \in \left[-1, \frac{1}{3}\right] \rightarrow \eta \in [1,0] \Rightarrow \eta = -\frac{1}{4}(3\xi - 1) \quad (46)$$

$$\int_\Gamma u_{ij}^*(p,Q) t_j(Q) d\Gamma(Q) =$$

$$\int_{-1}^{\frac{1}{3}} \frac{(3-4\nu)}{8\pi(1-\nu)\mu} \delta_{ij} \left\{ ln\left(\frac{1}{\left|\frac{1}{2}\left(\xi - \frac{1}{3}\right)\right|}\right) - \frac{1}{2} ln(l_e^2) \right\} + \frac{1}{8\pi(1-\nu)\mu} r_{,i} r_{,j} \psi(\xi) J d\xi \quad (47)$$

$$\int_{-1}^{\frac{1}{3}} \frac{(3-4\nu)}{8\pi(1-\nu)\mu} \delta_{ij} \left\{ ln\left(\frac{1}{\left|\frac{1}{2}\left(\xi - \frac{1}{3}\right)\right|}\right) \right\} \boldsymbol{\psi}(\xi) \boldsymbol{J} d\xi \rightarrow \int_0^1 \frac{(3-4\nu)}{8\pi(1-\nu)\mu} \delta_{ij} \left\{ ln\left(\frac{1}{\left|-\frac{2}{3}\right|}\right) + ln\left(\frac{1}{|\eta|}\right) \right\} \boldsymbol{\psi}(\xi) \boldsymbol{J} \left|-\frac{\mathbf{4}}{\mathbf{3}}\right| d\eta \quad (48)$$

$$\int_{-1}^{\frac{1}{3}} \frac{(3-4\nu)}{8\pi(1-\nu)\mu} \delta_{ij} \left(-\frac{1}{2}\right) l\, n(l_e^2)\, \boldsymbol{\psi}(\xi) \boldsymbol{J} d\xi \quad (49)$$

$$\int_{-1}^{\frac{1}{3}} \frac{1}{8\pi(1-\nu)\mu} r_{,i} r_{,j}\, \boldsymbol{\psi}(\xi) \boldsymbol{J} d\xi \quad (50)$$

3.2.3.2 $\left[\frac{1}{3}, 1\right]$ Interval Integration of Node 3

$$\xi \in \left[\frac{1}{3}, 1\right] \rightarrow \eta \in [0,1] \Rightarrow \eta = \frac{1}{2}(3\xi - 1) \quad (51)$$

$$\int_\Gamma u_{ij}^*(p,Q) t_j(Q) d\Gamma(Q) =$$

$$\int_{\frac{1}{3}}^{1} \frac{(3-4\nu)}{8\pi(1-\nu)\mu} \delta_{ij} \left\{ ln\left(\frac{1}{\left|\frac{1}{2}\left(\xi - \frac{1}{3}\right)\right|}\right) - \frac{1}{2} ln(l_e^2) \right\} + \frac{1}{8\pi(1-\nu)\mu} r_{,i} r_{,j}\, \boldsymbol{\psi}(\xi) \boldsymbol{J} d\xi \quad (52)$$

$$\int_{\frac{1}{3}}^{1} \frac{(3-4\nu)}{8\pi(1-\nu)\mu} \delta_{ij} \left\{ ln\left(\frac{1}{\left|\frac{1}{2}\left(\xi - \frac{1}{3}\right)\right|}\right) \right\} \boldsymbol{\psi}(\xi) \boldsymbol{J} d\xi \rightarrow \int_0^1 \frac{(3-4\nu)}{8\pi(1-\nu)\mu} \delta_{ij} \left\{ ln\left(\frac{1}{\left|\frac{1}{3}\right|}\right) + ln\left(\frac{1}{|\eta|}\right) \right\} \boldsymbol{\psi}(\xi) \boldsymbol{J} \left|\frac{\mathbf{2}}{\mathbf{3}}\right| d\eta \quad (53)$$

$$\int_{\frac{1}{3}}^{1} \frac{(3-4\nu)}{8\pi(1-\nu)\mu} \delta_{ij} \left(-\frac{1}{2}\right) l\, n(l_e^2)\, \boldsymbol{\psi}(\xi) \boldsymbol{J} d\xi \quad (54)$$

$$\int_{\frac{1}{3}}^{1} \frac{1}{8\pi(1-\nu)\mu} r_{,i} r_{,j}\, \boldsymbol{\psi}(\xi) \boldsymbol{J} d\xi \quad (55)$$

As mentioned earlier if calculation efficiency is to be sought, the expressions (49) and (50) in 3.2.3.1 and the expressions (54) and (55) in 3.2.3.2 can be obtained by applying a Gaussian numerical integration of the interval [-1, 1] simultaneously

3.2.4 Node 4 [-1,1] Interval Integration

$$r^2(p,Q) = \left(\sum_{i=1}^{2} N_i^m x_i - x_4\right) + \left(\sum_{i=1}^{2} N_i^m y_i - y_4\right) \quad (56)$$

$$= \left\{-\frac{1}{2}(\xi-1)\right\}^2 \{(x_1-x_4)^2 + ((y_1-y_4)^2)\} \geq 0 \quad (57)$$

$$\xi \in [-1,1] \longrightarrow \eta \in [1,0] \implies \eta = -\frac{1}{2}(\xi-1) \quad (58)$$

$$\int_\Gamma u_{ij}^*(p,Q)t_j(Q)d\Gamma(Q) =$$

$$\int_{-1}^{1} \frac{(3-4\nu)}{8\pi(1-\nu)\mu}\delta_{ij}\left\{ln\left(\frac{1}{\left|-\frac{1}{2}(\xi-1)\right|}\right) - \frac{1}{2}ln(l_e^2)\right\} + \frac{1}{8\pi(1-\nu)\mu} r_{,i}\, r_{,j}\, \boldsymbol{\psi}(\xi)\boldsymbol{J}d\xi \quad (59)$$

$$\int_{-1}^{-\frac{1}{3}} \frac{(3-4\nu)}{8\pi(1-\nu)\mu}\delta_{ij}\left\{ln\left(\frac{1}{\left|-\frac{1}{2}(\xi-1)\right|}\right)\right\}\boldsymbol{\psi}(\xi)\boldsymbol{J}d\xi$$

$$\longrightarrow \int_0^1 \frac{(3-4\nu)}{8\pi(1-\nu)\mu}\delta_{ij}\left\{ln\left(\frac{1}{|\eta|}\right)\right\}\boldsymbol{\psi}(\xi)\boldsymbol{J}|-\mathbf{2}|d\eta \quad (60)$$

$$\int_{-1}^{-1} \frac{(3-4\nu)}{8\pi(1-\nu)\mu}\delta_{ij}\left(-\frac{1}{2}\right) l\, n(l_e^2)\, \boldsymbol{\psi}(\xi)\boldsymbol{J}d\xi \quad (61)$$

$$\int_{-1}^{-1} \frac{1}{8\pi(1-\nu)\mu} r_{,i}\, r_{,j}\, \boldsymbol{\psi}(\xi)\boldsymbol{J}d\xi \quad (62)$$

This node is the last node of the element in which the singular integral occurs. However, in expression (60), pseudo Jacobian $|-\mathbf{2}|$ is different from the previous expression (27). As mentioned above, which is occurred because the mapping position between the original integration interval and the regular integration interval is inverted. This value is always positive.

3.3 Construction of A Linear Equation Set.

Eq. (63) shows the discretized boundary element equations, and eq (63) is generated for each node, forming Eq. (67), which is a linear equation for all unknowns. Finally, the elements of the diagonal matrix including $[C_{ij}]$ are calculated using formula (64), which is a general method used in ordinary BEM. Formula (64) is derived from the rigid body motion and is a useful expression that avoids the numerical error of integration performed at near strong singular point in the traction kernel, which is expressed by Eq. (22). In formula (64), $[H]^{ii}$ means diagonal matrixes where strong singularity occurs significantly. Formula (64) gives a value with sufficient accuracy for general problems, but cannot be used for open boundary and axisymmetric problems. The formula $[H]^{ii} = I - \sum_{\substack{j=1 \\ j\neq i}}^{NE} [H]^{ij}$ should be used. to analysis infinite domain. Expression (65) shows the matrix form of the basis function. The elements of matrix are zero except for the discretized boundary element that is currently integrated. Expression (66) is a formula for calculating Jacobian using mapping functions. Eq (67) is the index form of a linear equation set, which should be solved. The symbol NE means the Number of Elements.

$$\begin{bmatrix} C_{xx} & C_{xy} \\ C_{yx} & C_{yy} \end{bmatrix}_i \boldsymbol{u}_i + \sum_{j=1}^{NE} \int_{\Gamma(\xi)_j} \begin{bmatrix} T_{xx}^* & T_{xy}^* \\ T_{yx}^* & T_{yy}^* \end{bmatrix} [\psi(\xi)]_j \boldsymbol{J}d\xi \begin{Bmatrix} \vdots \\ \boldsymbol{u}_j \\ \vdots \end{Bmatrix} =$$

$$\sum_{k=1}^{NE} \int_{\Gamma(\xi)_j} \begin{bmatrix} U_{xx}^* & U_{xy}^* \\ U_{yx}^* & U_{yy}^* \end{bmatrix} [\psi(\xi)]_j \boldsymbol{J}d\xi \begin{Bmatrix} \vdots \\ \boldsymbol{t}_j \\ \vdots \end{Bmatrix} \quad (63)$$

$$[H]^{ii} = -\sum_{\substack{j=1 \\ j\neq i}}^{NE} [H]^{ij} \quad (64)$$

$$[\psi(\xi)]_j = \left[[\mathbf{0}] \cdots [\mathbf{0}] \begin{bmatrix} \psi_1^c & 0 & \psi_2^c & 0 & \psi_3^c & 0 & \psi_4^c & 0 \\ 0 & \psi_1^c & 0 & \psi_2^c & 0 & \psi_3^c & 0 & \psi_4^c \end{bmatrix}_j [\mathbf{0}] \cdots [\mathbf{0}] \right] \quad (65)$$

$$J = \frac{d\Gamma}{d\xi} = \sqrt{\left(\frac{d\sum_{i=1}^{2} N_i^m x_i}{d\xi}\right)^2 + \left(\frac{d\sum_{i=1}^{2} N_i^m y_i}{d\xi}\right)^2} \quad (66)$$

$$\sum_{j=1}^{NE} H_{ij}\, u_j = \sum_{j=1}^{NE} G_{ij} t_j \quad (67)$$

3.4 Internal Stresses and Boundary Stresses

The stresses of the internal points can be calculated using Eq. (68). The body force term has been omitted in eq. (68). S_{ijk}^* and D_{ijk}^* on the right side mean the third order tensors. Using the same procedure as for isoparametric elements, the mapping functions (eqs. (11, 12)) used in subparametric elements when calculating Jacobian are used.

$$\sigma_{ij}(p_{in}) + \int_\Gamma S_{ijk}^*(p_{in},Q)u_k(Q)d\Gamma(Q) =$$

$$\int_\Gamma D_{ijk}^*(p_{in},Q)t_k(Q)d\Gamma(Q) \quad (68)$$

The stresses at the boundary are calculated using Eqs. (69 ~74) and also using the mapping functions (Eqs. (11, 12)) used for the subparametric elements. The traction at the boundary is calculated for the tangent and normal vectors (Eq. (71)) and the value for the global coordinates is obtained using the coordinate transformation (Eq. (74)) [19]. The symbols used in these Eqs. (69~74) are as follows. The m_x, m_y are unit tangential vector components. The ε_{11} is the tangential strain. The local components of the traction vector, t_1, t_2 are defined as the tangential and normal

tractions to the boundary respectively. The M and M^T are transformation tensors of cartesian coordinate.

$$u_1(\xi) = \left\{\sum_{i=1}^{2} N_i(\xi)(u_x)_i\right\} m_x + \left\{\sum_{i=1}^{2} N_i(\xi)(u_y)_i\right\} m_y \quad (69)$$

$$\varepsilon_{11}(\xi) = \frac{1}{J(\xi)}\left[\left\{\sum_{i=1}^{2} \frac{\partial N_i(\xi)}{\partial \xi}(u_x)_i\right\} m_x + \left\{\sum_{i=1}^{2} \frac{\partial N_i(\xi)}{\partial \xi}(u_y)_i\right\} m_y\right] \quad (70)$$

$$\begin{bmatrix} t_1 \\ t_2 \end{bmatrix} = M \begin{bmatrix} t_x \\ t_y \end{bmatrix} \quad (71)$$

$$M = \begin{bmatrix} \cos\theta & \sin\theta \\ -\sin\theta & \cos\theta \end{bmatrix} \quad (72)$$

$$\begin{bmatrix} \sigma_{11} \\ \sigma_{22} \\ \sigma_{12} \end{bmatrix} = \begin{bmatrix} \frac{E}{1-v^2} & \frac{v}{1-v} & 0 \\ 0 & 1 & 0 \\ 0 & 0 & 1 \end{bmatrix} \begin{bmatrix} \varepsilon_{11} \\ t_2 \\ t_1 \end{bmatrix} \quad (73)$$

$$\sigma_{RS} = M_{iR}\sigma_{ij}M_{jS} = \boldsymbol{M^T \sigma\, M} \quad (74)$$

4. The Comparison of the Isoparametric and Subparamatric Element.

As mentioned above, the isoparametric elements are calculated by using the same function as the mapping function and the subparametric elements are calculated by setting the order of the mapping function lower than the basis function.

It is convenient to keep the mapping functions and base functions the same, and there is no reason why the two functions should be the same, and there is no reason to use functions of the same family. For example, the mapping functions can used as a Lagrange series, and the basis function can be used another function that can simulate the solution of the original partial or ordinary differential equations. In the case of DBEM, since the fundamental solution is multiplied by the coefficients of the basis functions, it can be seen that the basis functions and mapping functions are already different in a broad sense

The first difference between the subparametric elements and the isoparametric elements is the change in the calculation process due to the difference in the node between the mapping function N_i^m and the basis function ψ_i^c of the solution. That is, the order of the mapping function is low, the number of the nodes for the mapping functions is ever less than the number the nodes for the basis functions. Therefore, it is necessary to take a form different from the isoparametric element for the Jacobian calculation and the coefficient matrix integration of the DBEM.

Therefore, in Section 3.1, it is newly derived that formulas for integrating the kernel and the r value, the distance between the source and field points, to separate and calculate the singular value. Secondly, it is possible to eliminate the calculation of unnecessary mapping function when the straight line boundary is calculated, so that the calculation amount can be reduced and the calculation accuracy can be improved.

There is no difference in the number of integration points to be used, since it is governed by the degree of the base function, and there is no difference in the form of the eq (63), which is an explicitly shown discrete linear equation. The calculation procedure is the same except that the mapping functions are applied differently when calculating the boundary values and internal values corresponding to the post-processing.

5. Numerical Examples and discussion

5.1 The Simply Connected Region

As an example of verifying the proposed integral, we select cantilever beam, which is a representative problem of simply connected region as shown in Fig. 8. In the left part, the essential boundary condition (EBC) is applied as 0 and the natural boundary condition (NBC) of 1 N/mm is applied to the right free end. $E = 1000\, N/mm^2$, and $\nu = 0.25$. The basis function of the solution is cubic functions and the linear functions are used as mapping functions. The problem domain is a deep beam with a length of 100 mm and a height of 10 mm. The analysis results were compared with those of Plane stress, Timoshenko Beam, Euler Bernoulli Beam, quadratic isoparametric, and quadratic subparametric elements. In Fig. 9.,  are nodes in which mapping function and a basis function exists at the same time. Nodes  are pure basis node and Nodes are Fixed EBC.

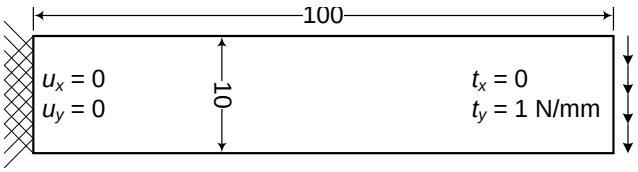

Fig. 8. The simply connected region (cantilever Beam)

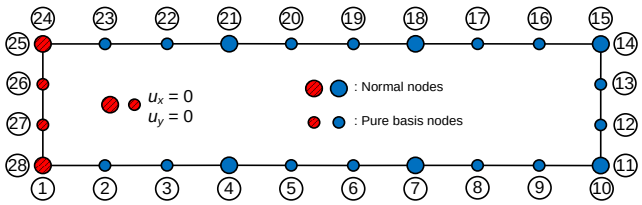

Fig. 9. The discretization for CSDBEM analysis (8 elements, 28 nodes)

In Fig. 9., it is represented that the discretization model using 8 elements. Fig. 10. shows the solution at the center of the beam height. The results of the CSDBEM are shown below the Plane stress solution and the Euler Beam solution. Therefore, we can conclude that the analysis accuracy is guaranteed and the kernel integrals are correct.

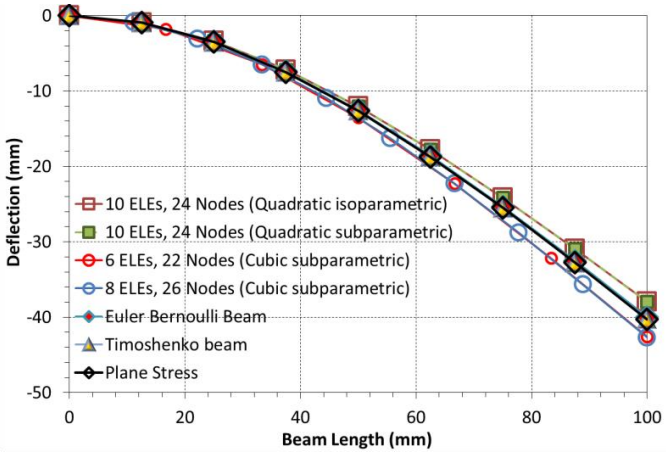

Fig. 10. Results of isoparametric, subparametric DBEM element and others

To verify that the overall deformed shape is calculated correctly, Fig. 11. shows the final variant form for both models. The results of analysis are normal. Fig. 12. shows the error of the analysis for the plane stress solution according to each position. The error decreases at the Beam ends. This is because the error ratio decreases as the deflection value i.e. reference value increases toward the end portion. Since the anomalous value is not particularly shown, the analysis result is also valid in all areas. The validity of CSDBEM was verified through Fig. 10, 11, 12, and the following examples were performed based on inductive reasoning.

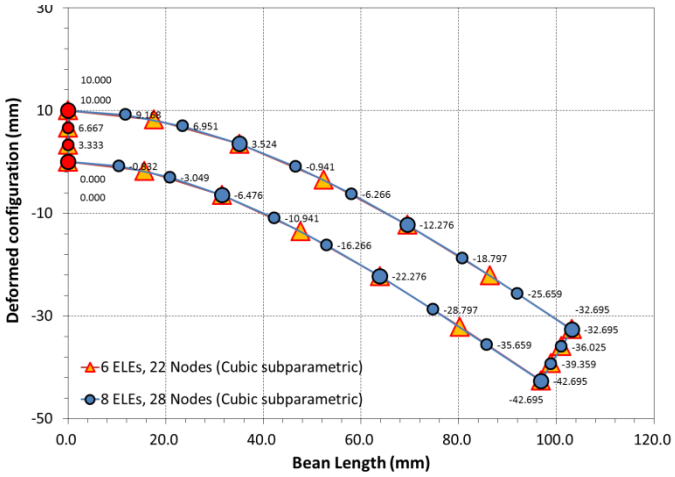

Fig. 11. Deformed configuration of cubic subparametric 6 and 8 elements

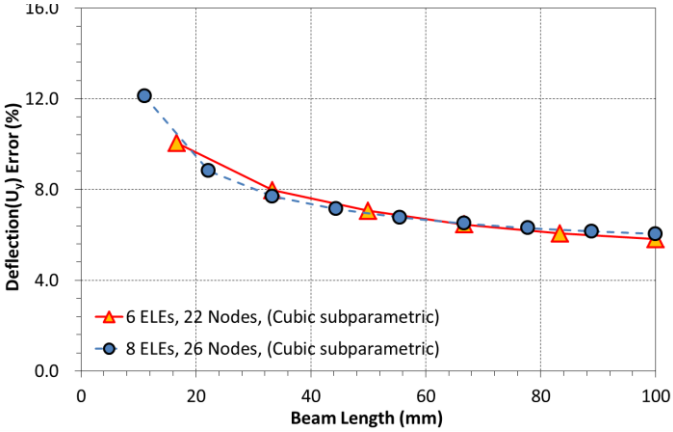

Fig. 12. u_y Error (%) about length of cantilever

5.2 The Multiply Connected Region

The outer boundary and the inner hole problem, which are representative examples of the multiple connection regions is analyzed. This domain represents the box culvert shape. The discretization directon of internal boundary was set to clockwise. The boundary conditions are shown that the EBC selected the fixed on the left side and applied NBC 1 N/mm on the right side, as shown in Fig. 13. The material constants were set to $E = 1000\,N/mm^2$, $\nu = 0.25$ as in the previous example.

The reason for selecting NBC as the right side load and the EBC as the left side fixed is to verify the validity of the proposed method for the integration of the subparametric elements through the model with the clear deformation. This problem is somewhat different to 1/4 L-shape domain usually analyzed because of left side wholly fixed boundary condition as mentioned in pervious paragraph. It has been shown that one of the discretization of CSDBEM to analyze the problem in Fig. 14.

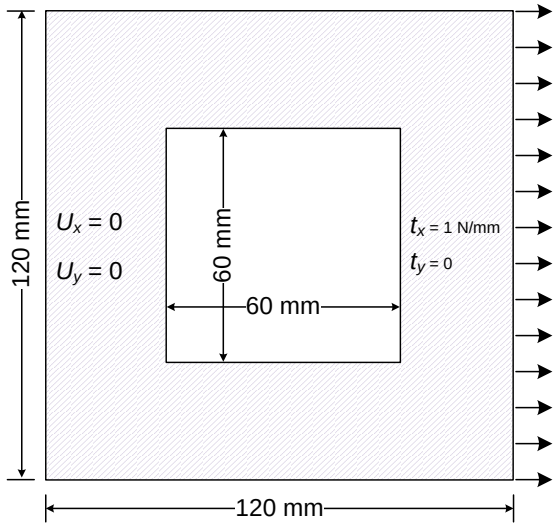

Fig. 13. The multiply connected region (cut out plate)

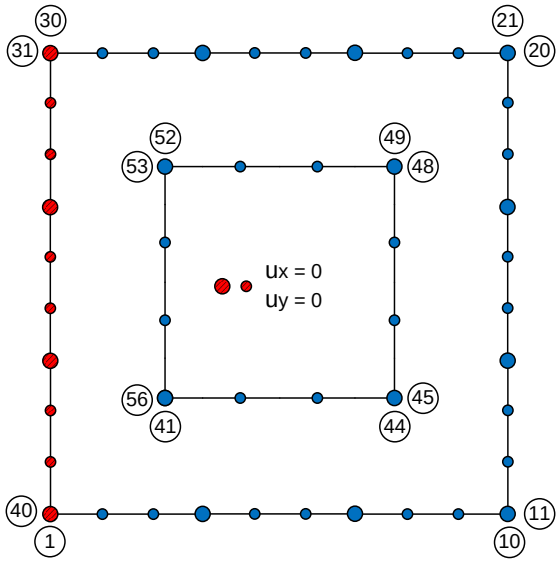

Fig. 14. The discretization of CSDBEM analysis (16 elements 56 nodes)

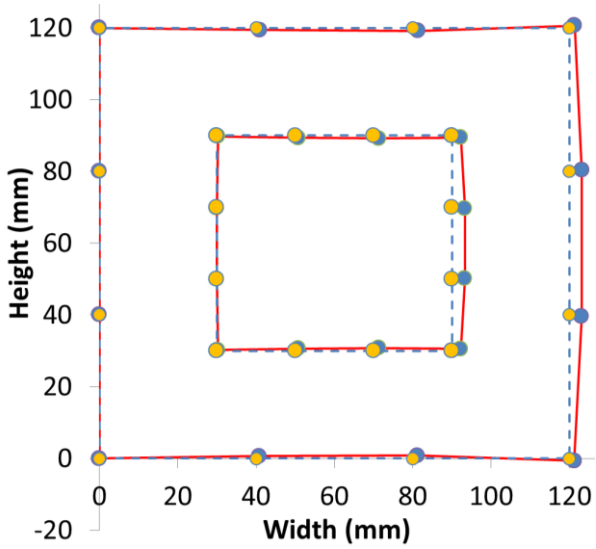

Fig. 15. The deformed, original domain (4 elements, 32 nodes)

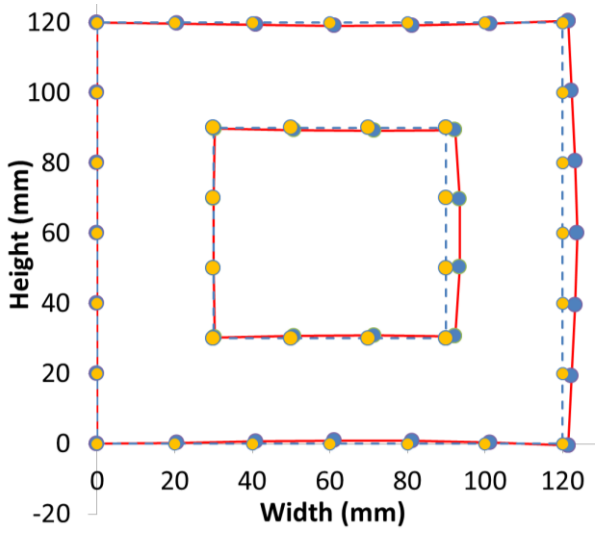

Fig. 16. The deformed, original domain (12 elements, 44 nodes)

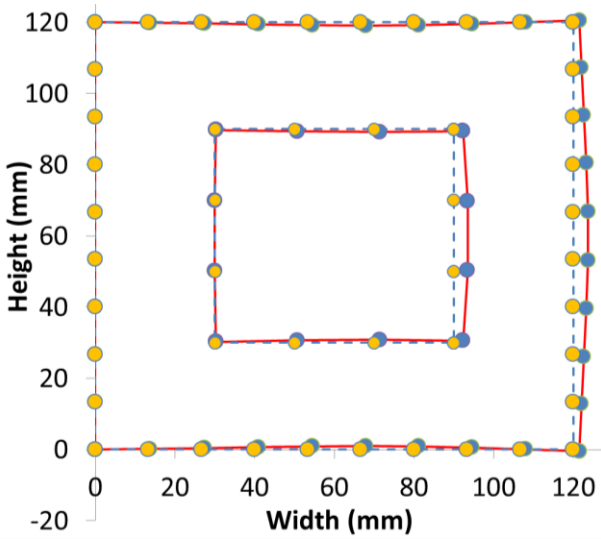

Fig. 17. The deformed, original domain (16 elements, 56 nodes)

To verify that the overall deformed shape was properly calculated, Deformation diagrams are shown in Figs. 15, 16, 17. The figures are amplified to show deformed configurations clearly. As can be seen from the whole figures, the deformed shape shows well when the load is applied to the right side. It can be seen that the reduction phenomenon of the central part appears well.

Figs. 18, 19, 20. show stresses contour of σ_{xx}, σ_{yy}, σ_{xy} in the undeformed domain. Symmetric stresses contour appear in Figs. 18, 19. At the re-entrant corner of upper right part inside empty space, compressive stress occurred. It is shown that the tensile stress occurs at the coordinates (60, 30), (60, 90) and (115, 60). Antisymmetric stress distribution occurs in the Fig. 20. This distribution can be taken for granted due to the nature of the shear stress. Considering the stress distribution, the calculation is accurate.

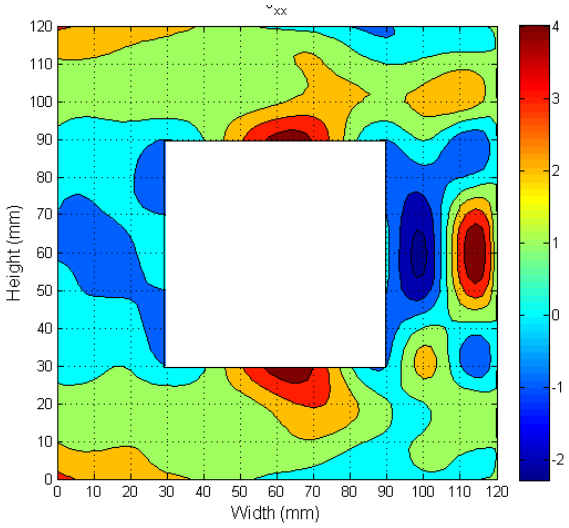

Fig. 18. σ_{xx} contour diagram

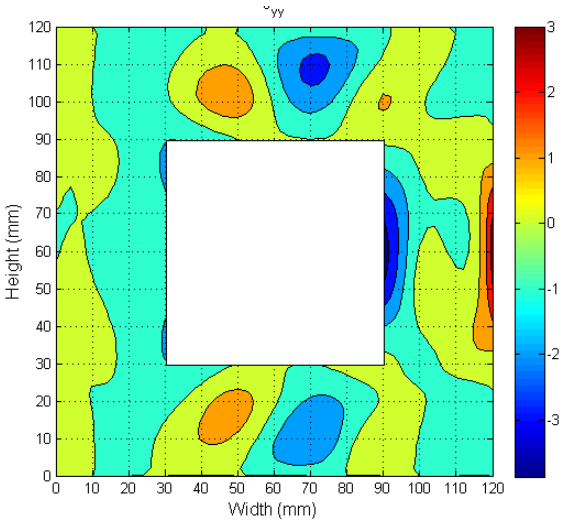

Fig. 19. σ_{yy} contour diagram

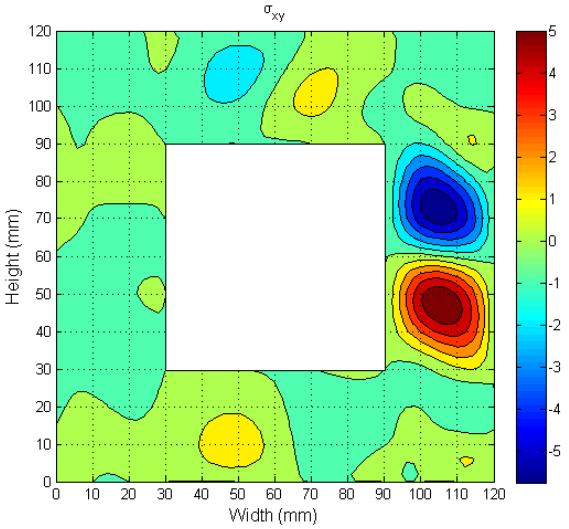

Fig. 20. σ_{xy} contour diagram

$u_x(x = 120,\ y = 90)$ calculated by cubic subprametric and linear element were plotted about DOFs. u_x of cubic subparametric elements 66 DOFs is similar to that of Linear elements 114 DOFs. If more degree of freedom is used, the solutions will converge gradually in both cases. In addition, a sharp increase of graphs is not found because of the displacement solution in Fig. 21.

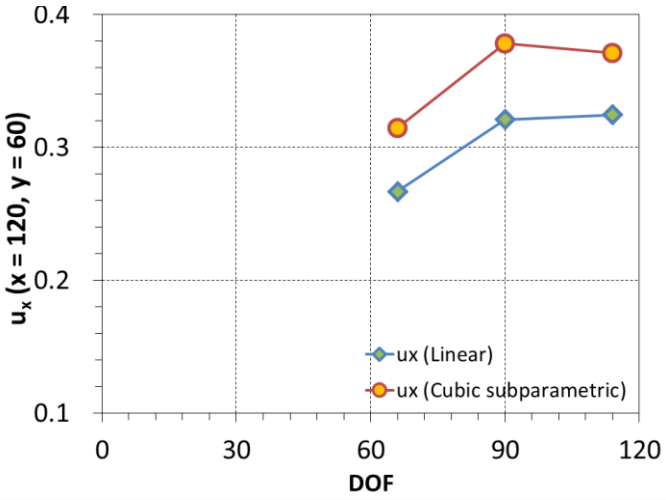

Fig. 21. u_x Linear and Cubic subparametric elements about DOFs

σ_{xx} of upper side of inner square are plotted in the Fig 22.. In the vicinity of the point$(x = 90,\ y = 90)$ where stress concentration occurs, σ_{xx} of cubic supbparametric elements is sharply increase but that of linear elements is increase gradually. If stresses don't increase in the domain, which stress should increase sharply, additional degree of freedoms should be deployed or the place of nodes that already used to analysis should be moved. The effectiveness of degree of freedom will be discussed in the following example.

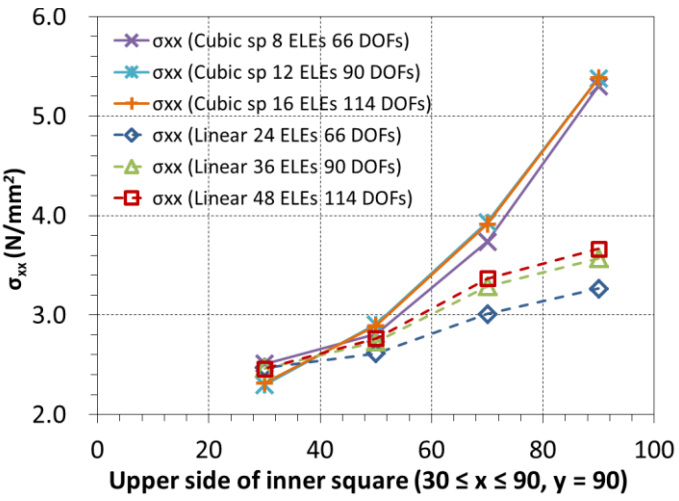

Fig. 22. σ_{xx} about DOFs along upper side of inner square $(30 \le x \le 90,\ y = 90)$

5.3 The Double Edge Notched Plate

Finally, a double notched plate was selected as a preliminary example for application to fracture mechanics. Fig. 23. shows the overall shape, Fig. 24. shows the 1/4 domain[18]. The EBCs are represented by symmetry axes. The notch length was chosen to be 1/3 of the width. $\sigma = 1\ N/mm^2$ $(t_y = 1\ N/mm)$ has been applied to the upper side of the domain.

Fig. 25. shows the most typical stress state σ_{yy} in the deformed configuration. Fig. 26. is σ_{xy}, Fig. 27. denotes σ_{xx}. Fig 25 is the deformed configuration that has been amplified 100 times over the original deformed configuration derived by calculation to observe it in detail. Fig. 28. represents the shape of the solution as vectors. This vector marker is very useful to fix the code written for the first time because the peculiarity of the solution can be seen with a flow picture.

In the Figs. 25, 26, 27, Eqs. (66-72) and linear mapping are used to perform post-processing calcuations. The shape of the strip is well represented in the deformed configuration and the stress contour diagrams. In order to clearly observe the change of stress, σ_{yy}, which is the stress in the same direction as the applied load, is plotted as a vertical graph in Fig. 29., It can be seen that the stress rises sharply at the start of the crack.

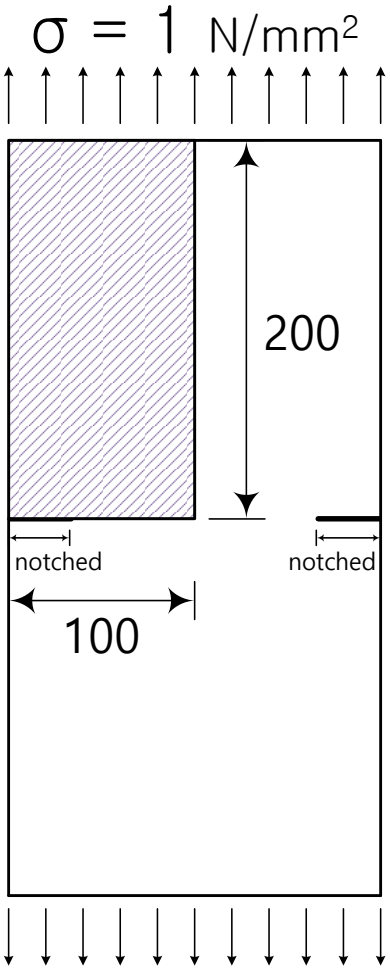

Fig 23. Double crack plate and 1/4 domain

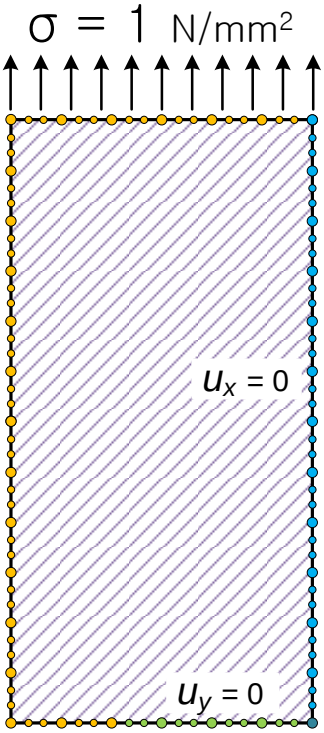

Fig. 24. The discretization for CSDBEM analysis

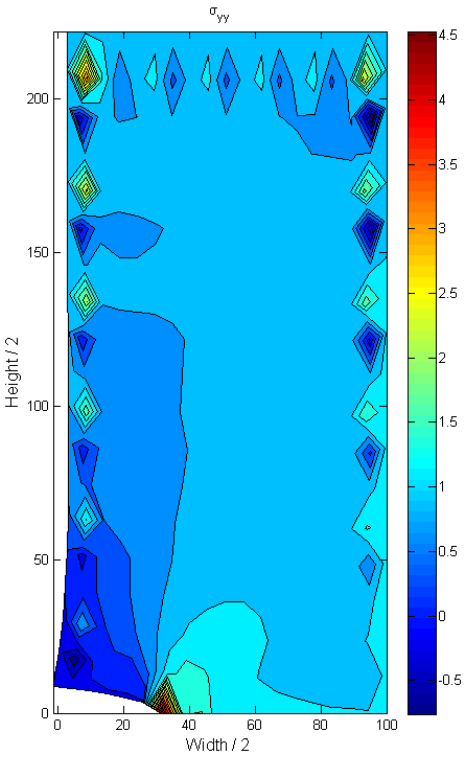

Fig. 25. σ_{yy} contour diagram in the deformed domain

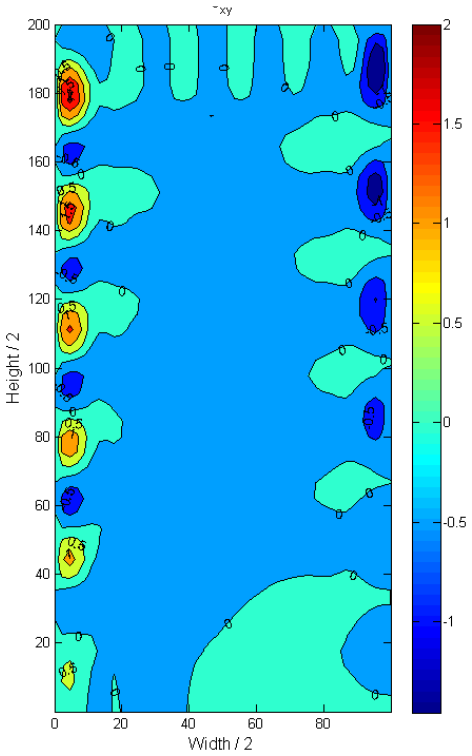

Fig. 26. σ_{xy} contour diagram

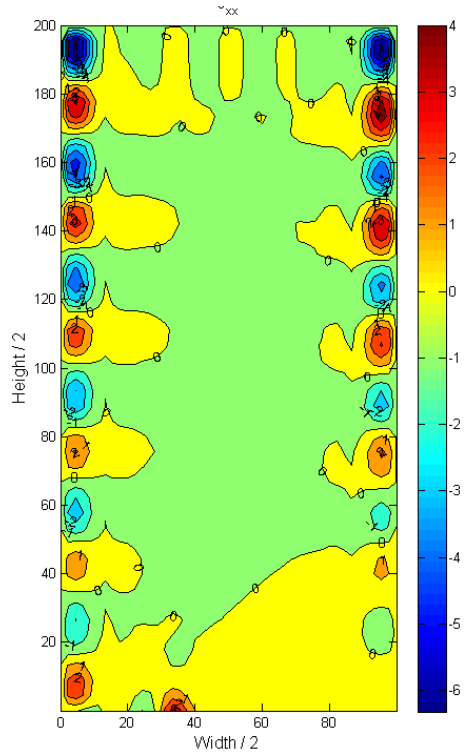

Fig. 27. σ_{xx} contour diagram

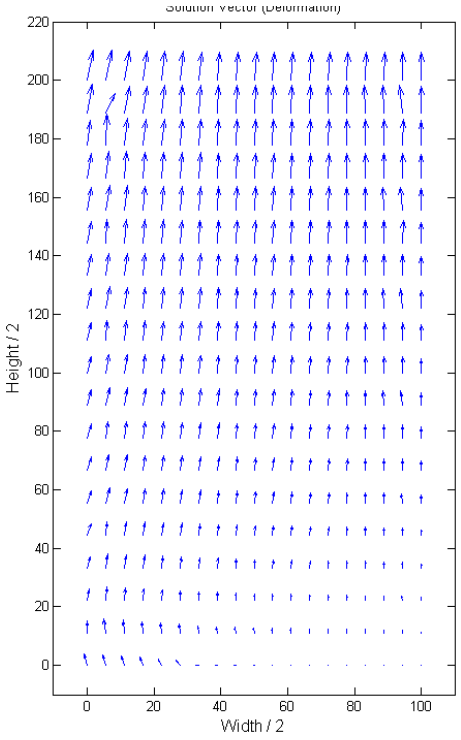

Fig. 28. u_x and u_y displacement vector

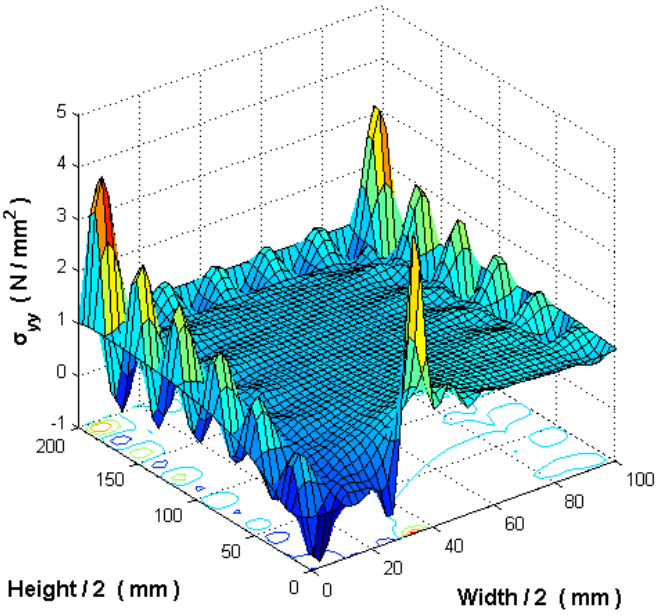

Fig. 29. σ_{yy} stress surface plot

$$\sigma_{yy} = \frac{K_I}{\sqrt{2\pi r}} cos\frac{\theta}{2}\left(1 + sin\frac{\theta}{2} sin\frac{3\theta}{2}\right) \quad (75)$$

In the Figs. 30, 31, the displacement values of the linear and cubic subparametric elements are shown for degrees of freedoms. It can be seen that as the degree of freedoms increases for both elements, it approaches a similar point. However, any notable differences cannot be found in the convergence pattern between linear and cubic

subparametric elements.

Figs. 32, 33, σ_{xx} and σ_{yy} are shown for degrees of freedom at $y = 0$ position. In this graph, a clear feature can be seen. More specifically, it can be seen that the stress values calculated by the cubic subparamatric from the small DOF number to the many DOF numbers exist above the stress value calculated by Linear. The same phenomenon as shown in the Figs. 32, 33, can be seen. It is believed that the stress is significantly enhanced by the cubic subparametric elements in the stress intensity region rather than the displacement.

There are the third order tensors S^*_{ijk} and D^*_{ijk} consist of the values of $\frac{1}{r}, \frac{1}{r^2}$. In eq. (68) that used to calculate the stresses. Therefore, the value of stresses rises rapidly as the value of r decreases. It can be said that the increase is more serious than displacements. When this value is used as integrands, strong singularity and hyper singularity appear, respectively [11, 12]. In conclusion, the cubic basis function is much more suitable than the linear basis function in the problem of stress intensity.

In addition, the stress distribution near the crack in the OPENING MODE is given by eq. (75) for σ_{yy}. In eq (75), K_I is the stress intensity factor. The denominator of eq. (75) consists of the distance value (r) to the location of the crack tip and the stress under consideration. When this distance value approaches 0, the stress value becomes ∞. Therefore, the analytical value should be much larger than the applied load. Since it is theoretically ∞, it is difficult to set a limit. If the elements are subdivided for this model, the value will rise further when looking at the trend of the graph. For the stresses σ_{xx} and σ_{xy} the composition of the equations is the same [18]

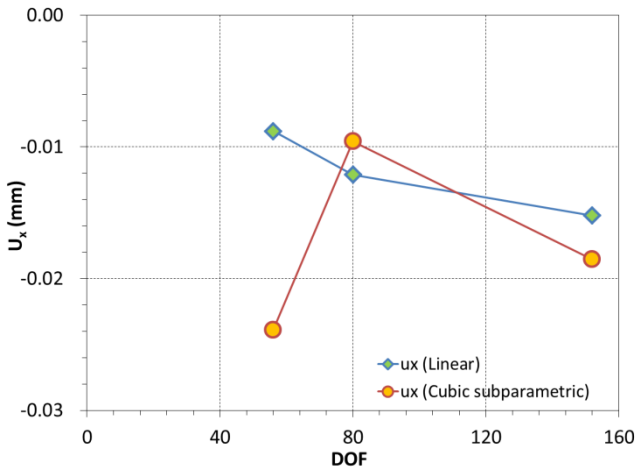

Fig. 30. u_x Linear and Cubic subparametric elements about DOFs at $x = 0, y = 0$

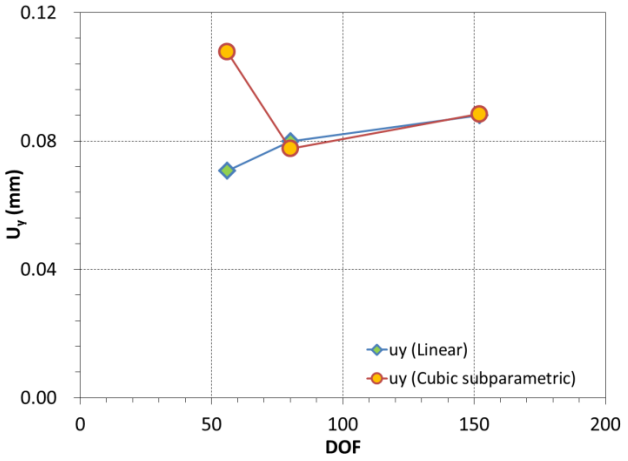

Fig. 31. u_y Linear and Cubic subparametric elements about DOFs at $x = 0, y = 0$

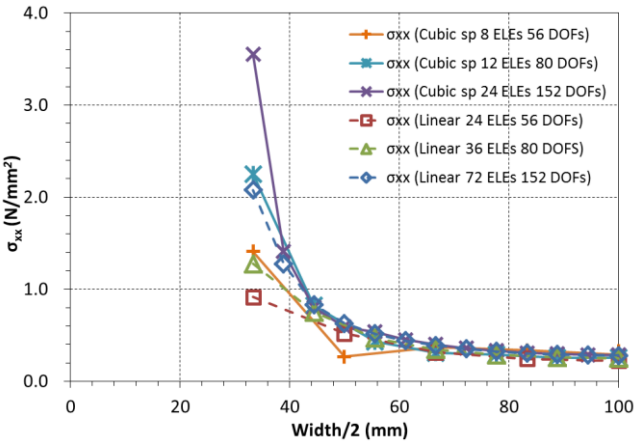

Fig. 32. σ_{xx} along $y = 0$ about DOFs along width

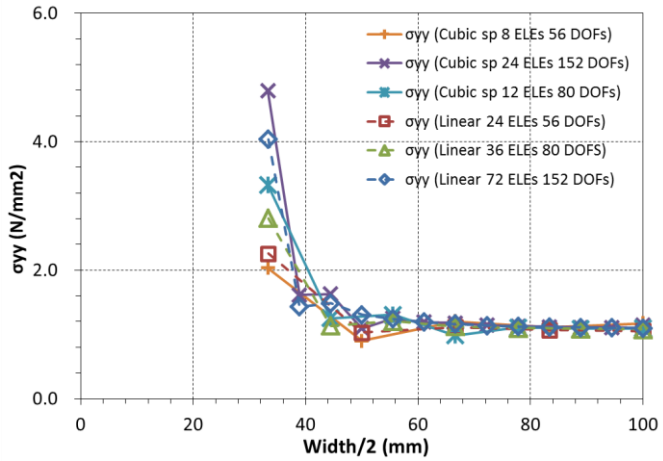

Fig. 33. σ_{yy} along $y = 0$ about DOFs along width

By simplifying the Figs, 34 and 35 show stress values at crack tip according toπ DOFs. The gradients of regression equations in Figs. 34, 35, have been calculated. The gradients can be recognized as the convergence speed in this problem. The gradient of cubic subparametric element is approximatively one and a half as much as that of linear element as shown in table. 1.

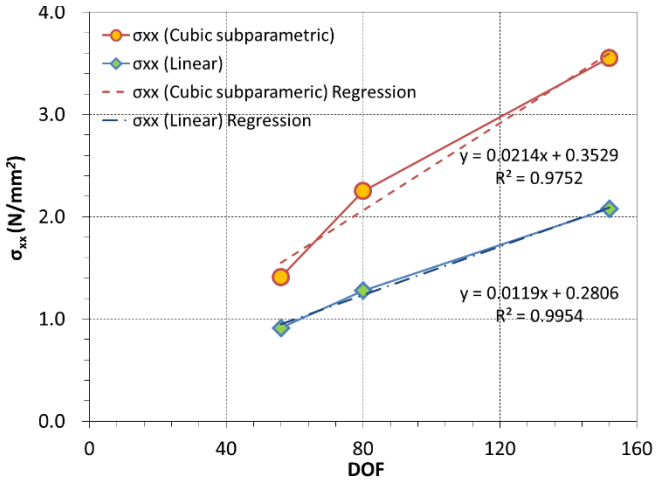

Fig. 34. σ_{xx} Results of Linear and Cubic subparametric elements about DOFs at crack tip

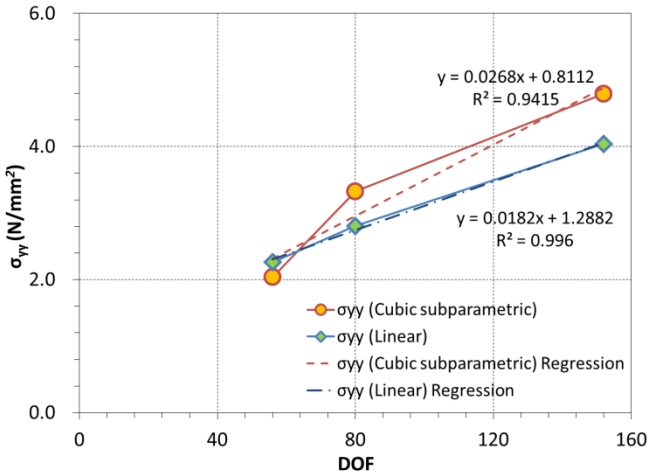

Fig. 35. σ_{yy} Results of Linear and Cubic subparametric elements about DOFs at crack tip

Table 1. The comparison of gradients between cubic subparametric and Linear element

Element type	Gradients	
	σ_{xx}	σ_{yy}
Cubic subparametric	0.0214	0.0268
Linear	0.0119	0.0182
The Ratio of Gradients	1.7983	1.4725

This means that cubic subparametric elements approach to the solution of problem faster than linear elements considering using the same degree of freedoms. This is somewhat natural because the degree of freedoms used as variables are calculated in the cubic polynomial terms which perform a lot of floating point operations. However, both convergence rates will decrease gradually. It is not possible to predict the progressive decrease phenomena using the regression lines. The gradual reduction of convergence rates will be discussed using the normalization concept of convergence rates in the following.

The Contribution ratios of DOF to stress convergence gradient are plotted in Figs. 36, 37. They also show that the contribution of cubic subparametric elements to convergence rates is higher than linear elements. These results can be inferred from Figs. 34, 35.

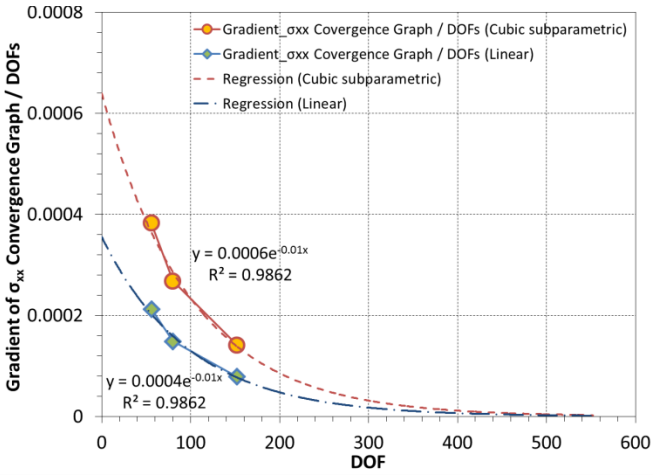

Fig. 36. Contribution ratio of DOFs to σ_{xx} convergence gradient (Normalized gradient per DOF)

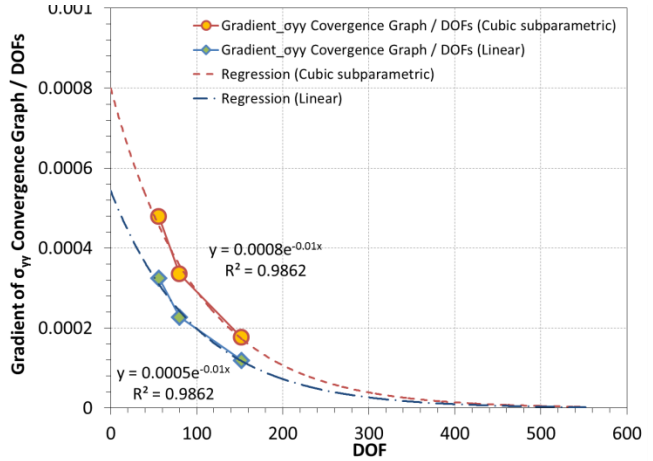

Fig. 37. Contribution ratio of DOF to σ_{yy} convergence gradient (Normalized gradient per DOF)

The vertical axes are gradients of σ_{xx} σ_{yy} convergence graph in Figs 36, 37. If the graph is larger than the horizontal axis, it means that the solution is still converging at the corresponding degree of freedom. Also, it means that the upper graph is converging faster than the lower graph. As can be seen in Figs. 36, 37, the cubic subparametric element graph is above to the linear element

graph.

If so, the question arises as to when convergence can proceed. It can also be seen schematically by extrapolated curves at the back of Figs. 36, 37. The graphs of cubic subparametric and linear element nearly approach contact to the horizontal axis. If the graphs close on the horizontal axis, convergence no longer occurs. This method has been applied to the problem of stress intensity, but it is expected that similar tendencies will be observed when applied to general problems.

Table 2. The Extrapolation values of Gradient of σ_{xx} Convergence Graph / DOFs

DOFs	Cubic subparametric $0.0006e^{-0.01x}$	Linear $0.0004e^{-0.01x}$	Difference	$\frac{\text{Difference}}{\text{Difference of DOF 1}}$(%)
1	5.9403E-04	3.9602E-04	1.9801E-04	100.00
460	6.0311E-06	4.0207E-06	2.0104E-06	1.0153
461	5.9711E-06	3.9807E-06	1.9904E-06	1.0052
462	5.9117E-06	3.9411E-06	1.9706E-06	0.9952
463	5.8529E-06	3.9019E-06	1.9510E-06	0.9853

Table 3. The Extrapolation values of Gradient of σ_{yy} Convergence Graph / DOFs

DOFs	Cubic subparametric $0.0008e^{-0.01x}$	Linear $0.0005e^{-0.01x}$	Difference	$\frac{\text{Difference}}{\text{Difference of DOF 1}}$(%)
1	4.9502E-04	5.9403E-04	9.9005E-05	100.00
460	5.0259E-06	6.0311E-06	1.0052E-06	1.0153
461	4.9759E-06	5.9711E-06	9.9518E-07	1.0052
462	4.9264E-06	5.9117E-06	9.8528E-07	0.9952
463	4.8774E-06	5.8529E-06	9.7548E-07	0.9853

It is shown that difference between gradient of σ_{xx}, σ_{yy} convergence graphs in the table 2, 3. The percentage of the gradient difference for the gradient of the degree of freedom 1 goes down to less than 1 % from the degree of freedom 462. Therefore, the convergence speed between the cubic subparametric element and the linear element is not much different from the degree of freedom of 460 or more.

6. Conclusion

In this paper, we investigated the kernel integration method of cubic subparametric elements and developed the formulas. In general, subparametric elements are effective from a calculation point of view because lower order mapping functions are used. The proposed integration method and induced formulas are applied to several examples to verify the performance. The several examples are the simply connected region, the multiply connected region and the stress intensity problem. The proposed numerical integration technique has yielded stable results.

Also the performance of cubic subparmetric boundary elements had been investigated using the gradient of stresses convergence graph. In other words, the effectiveness of degree of freedom is discussed through the examples. On the whole, a CSDBE is more effective than a linear boundary element using same the number of degree of freedoms. Considering the polynomial order used in the formulation, this result stands to reason. In other words, If mapping functions are equal in each kind of elements, the number of degree of freedoms and polynomial order are remaining factors that affect solution quality. Under this state of things, if the same number of degree of freedom is used in analyses, the influence of polynomial order appears through the efficiency of one degree of freedom. Through the examples, it is shown that efficiency of a degree of freedom has improved according to polynomial order.

Meanwhile, the integration method proposed in this paper can also be used when nodes exist at any position inside the element. That is, it is an indispensable calculation method for integrating the kernel when implementing the *R*-Adaptive (Node relocation adaptive) method that locally changes the location of the nodes, in which stress intensity occurs. Physically speaking, fields where adaptive analysis is needed are typically stress intensity regions. Usually, better solutions compared with FEM can be obtained because of the high accuracy characteristics of the BEM. In these cases, The Adaptive analysis will be a way to efficiently allocate computational resources which limited physically. Also this integration technique is material to realize the discontinuous boundary element which used to satisfy the Hölder continuity[11].

Finally, since it had been clarified that the kernel integration method mentioned in the introduction, it will increase the accessibility of users interested in DBEM. The integral calculation can be reproduced by only the contents of this paper. Although these contents describe the integration of cubic subparametric elements, the same method can be applied to the iosparametric quadratic element, the isoparametric cubic element and the discontinuous elements that nodes are in the inside of elements.

Reference

[1] T.J.R. Hughes, A. Reali, G. Sangalli, "Efficient quadrature for NURBS-based isogeometric analysis", Comput. Methods Appl. Mech. Engrg. 199 (5–8) (2010) 301–313.

[2] T.J.R. Hughes, J.A. Cottrell, Y. Bazilevs, "Isogeometric analysis: CAD, finite elements, NURBS, exact geometry and mesh refinement", Comput. Methods Appl. Mech. Engrg. 194 (39–41) (2005) 4135–4195.

[3] F. Auricchio, L.B. Da Veiga, T.J.R. Hughes, A. Reali, G.

Sangalli, "Isogeometric collocation methods", Math. Models Methods Appl. Sci. 20 (11) (2010) 2075–2107.
[4] R.N. Simpson, S.P.A. Bordas, J. Trevelyan, T. Rabczuk, "A two-dimensional Isogeometric Boundary Element Method for elastostatic analysis", Comput. Methods Appl. Mech. Engrg. 209–212 (2012) 87–100
[5] Luigi Iuspa, Pietro Fusco, Eugenio Ruocco, "An improved GPU-oriented algorithm for elastostatic analysis with boundary element method", Computers and Structures, vol. 146, pp. 105–116. January 2015, https://doi.org/10.1016/j.compstruc.2014.08.009
[6] Crim, "Deveopment of The boundary element method and combination with the finite element method in *p*-Version", Ph.D. Dissertation, Vanderbilt University, 1992
[7] P. K. Basu, A. B. Jorge, S. Badri, and J. Lin, "Higher-order modeling of continua by finite-element, boundary-element, meshless, and wavelet methods", Computers & Mathematics with Applications, vol. 46, no. 1, pp. 15–33, 2003.
[8] M. M. Perez, L. C. Wrobel "An Integral-Equation Formulation for Anisotropic Elastostatics", Journal of Applied Mechanics, DECEMBER 1996. vol. 63. 891-902
[9] R.N.L. Smith, "Direct Gauss quadrature formulae for logarithmic singularities on isoparametric elements", Eng. Anal. Bound. Elem. 24, 161–167, 2000
[10] JOHN A. CROW, "QUADRATURE OF INTEGRANDS WITH A LOGARITHMIC SINGULARITY", mathematics of computation, vol 60, no. 201, 297-301, January, 1993
[11] PORTELA AND M. H. ALIABADI, "THE DUAL BOUNDARY ELEMENT METHOD: EFFECTIVE IMPLEMENTATION FOR CRACK PROBLEMS", Int J Numer Methods Eng, vol. 33, 1269-1287 (1992)
[12] JUKKA TUHKURI, "DUAL BOUNDARY ELEMENT ANALYSIS OF CLOSED CRACKS", Int J Numer Methods Eng , vol. 40, 2995-3014 (1997)
[13] C. A. Brebbia, J.C.F. Telles, L.C. Wrobel, "BE Techniques Theory and Applications in Engineering", Springer-Verlag, 1984
[14] A. El Zafrany, "Techniques of the boundary element method", ELLIS HORWOOD, 1993
[15] Mohammed ameen, "boundary element analysis theory and programming", CRC press, 2000
[16] A.A. Becker "The Boundary Element Method in Engineering A complete course", McGRAW-HILL, 1992
[17] J. N. Reddy, "An introduction to the finite element method", McGRAW-HILL, 2nd edition, 1993.
[18] Hiroshi Tada, paul C. paris, george R. irwin , "The stress analysis of cracks hand book", Del Research corporation Hellertown, Pennsylvania 1973
[19] A.J.M. Spencer "Continuum mechanics", Longman mathematical text, 1980